ACCOUNTS of chemical research

Article

pubs.acs.org/accounts

Size, Dimensionality, and Strong Electron Correlation in Nanoscience

Louis Brus*

Department of Chemistry, Columbia University, New York, New York 10027, United States

CONSPECTUS: In electronic structure theory, electron−electron repulsion is normally considered only in an average (or mean field) sense, for example, in a single Hartree−Fock determinant. This is the simple molecular orbital model, which is often a good approximation for molecules. In infinite systems, this averaging treatment leads to delocalized electronic bands, an excellent description of bulk 3D sp^3 semiconductors. However, in reality electrons try to instantaneously avoid each other; their relative motion is correlated. Strong electron−electron repulsion and correlation create new collective states and cause new femtosecond kinetic processes. This is especially true in 1D and 2D systems. The quantum size effect, a single electron property, is widely known: the band gap increases with decreasing size. This Account focuses on the experimental consequences of strong correlation. We first describe $\pi-\pi^*$ excited states in carbon nanotubes (CNTs). To obtain the spectra of individual CNTs, we developed a white-light, right-angle resonant Rayleigh scattering method. Discrete exciton transitions dominate the optical absorption spectra of both semiconducting and metallic tubes. Excitons are bound neutral excited states in which the electron and hole tightly orbit each other due to their mutual Coulomb attraction. We then describe more generally the independent roles of size and dimensionality in nanoelectronic structure, using additional examples from graphene, *trans*-polyacetylene chains, transition metal dichalcogenides, organic/inorganic Pb iodide perovskites, quantum dots, and pentacene van der Waals crystals. In 1D and 2D chemical systems, the electronic band structure diagram can be a poor predictor of properties if explicit correlation is not considered. One- and two-dimensional systems show quantum confinement and especially strong correlation as compared with their 3D parent systems. The Coulomb interaction is enhanced because the electrons are on the surface. One- and two-dimensional systems can exhibit essentially molecular properties even though they are infinite in size. Zero-dimensional Qdots show quantum confinement and modest electron correlation. Correlation is weak in 3D bulk semiconductors. Strongly correlated electronic states can behave as if they have fractional charge and effectively separate the spin and charge of the electron. This is apparent in the "soliton" state of polyacetylene, the fractional charge quantum Hall state of graphene, and the Luttinger electrical conductivity of metallic CNTs.

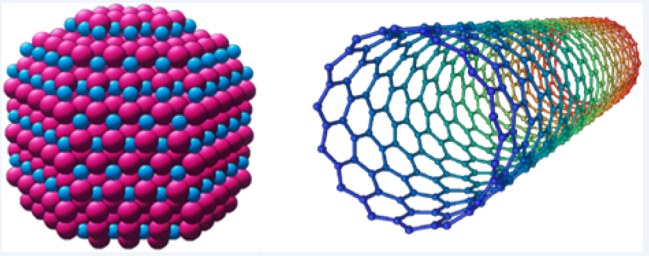

SINGLE CARBON NANOTUBES OBSERVED BY RAYLEIGH SCATTERING

Iijima's 1991 discovery of sp^2 hybridized single wall CNTs was a seminal event in nanoscience.[1] It focused attention on extended π electron systems in nearly one-dimensional (1D) CNTs (Figure 1) and eventually in 2D graphene sheets (Figure 2). The CNT family became especially intriguing because it was quickly realized that some would be metals while others would be semiconductors.[2,3] These extended π systems have no surface states and show very high carrier mobilities. The subsequent worldwide research explosion led to the 2004 discovery by Geim, Novoselov, and co-workers[4] of an effective way to exfoliate single graphene sheets.

My colleagues and I began to think about CNT excited electronic states. There are hundreds of structurally different CNTs, and thus there is a strong reason to experimentally study single nanotubes. At this time we were exploring single molecule and single quantum dot luminescence using far-field confocal techniques.[5,6] Because luminescence is a zero background method, individual molecules and quantum dots emitting in the visible with unity quantum yields are relatively easy to detect. However, metallic CNTs do not luminescence. Smalley, Weisman, and co-workers discovered that micelle-solubilized semiconductor CNTs emit,[7] but the emission was in the near-infrared with low quantum yield. They observed good heterogeneous ensemble emission spectra, but it would be hard to detect single tubes.

It also seemed daunting to try to directly measure the optical absorption spectrum of one tube, because this would necessitate the measurement of light attenuation at perhaps 1 part in 10^7. We thought about the possibility of elastic Rayleigh scattering detection. In molecular spectroscopy, one would never consider Rayleigh scattering, because the Rayleigh cross section is far smaller than the absorption cross section. However, Rayleigh scattering is a coherent process that scales as the square of an object's size, compared with absorption, which typically scales linearly with size. As size increases, Rayleigh scattering increases faster than optical absorption. Thus, nanoscale objects might have detectible Rayleigh scattering; indeed, Ag nanoparticle Rayleigh (plasmon) scattering is easily observed. At this time, we were using

Received: April 30, 2014
Published: August 13, 2014

   dx.doi.org/10.1021/ar500175h | *Acc. Chem. Res.* 2014, 47, 2951−2959

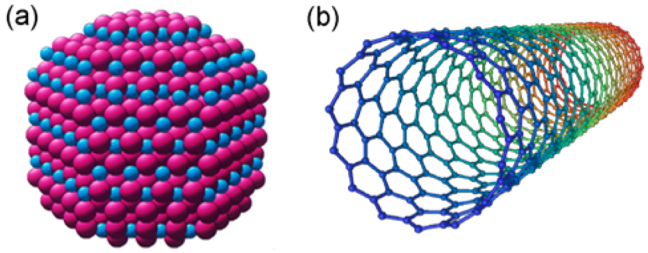

Figure 1. (a) CdSe nanocrystal without ligands: Se atoms red and Cd atoms blue. (b) Carbon nanotube.

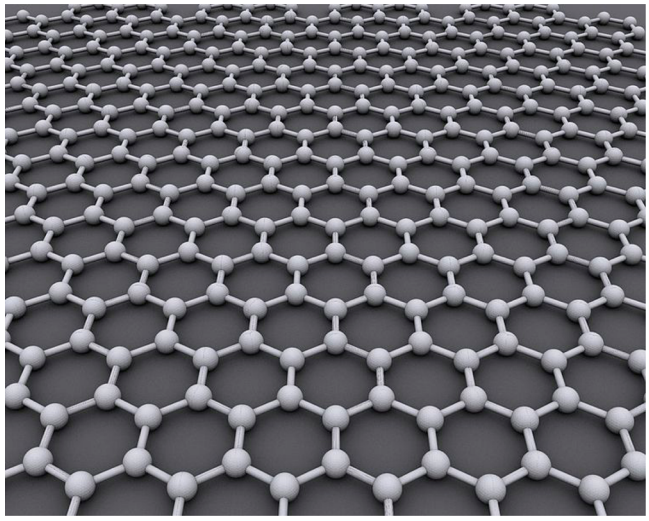

Figure 2. Graphene.

white light Rayleigh scattering to study single molecule surface enhanced Raman scattering (SERS) in Ag colloids.[8,9]

Rayleigh scattering would detect both metallic and semiconducting tubes. The Rayleigh spectrum would essentially mimic the absorption spectrum, because the Rayleigh cross section has a resonance at optical absorption energies. Moreover, right angle Rayleigh scattering is a zero background technique like luminescence. With Zhonghua Yu in 2001, we set out to measure CNT Rayleigh scattering.[10] Matt Sfeir observed individual tubes using a high brightness, supercontinuum light source, in close collaboration with Feng Wang, Tony Heinz, Jim Hone, and colleagues.[11,12] Combining Raman, TEM and Rayleigh measurements on single tubes was especially informative (Figure 3).[13−15]

The Rayleigh spectra showed discrete, molecule-like excited states for both metallic and semiconducting tubes. The metallic tube spectra are far different than the featureless broad spectra of bulk metals such as Cu or Pt. We focused on trying to understand CNT excited electronic states and strong correlation more generally.[16]

CARBON NANOTUBES AND GRAPHENE

In 1997, Ando predicted pronounced exciton effects in semiconducting CNTs due to strong electron correlation.[17] Let us ignore correlation for the moment. CNTs show quantized, discrete electron motion for π electrons going around the circumference; such electrons need to interfere constructively with themselves in order to create a stationary state. Thus, only discrete values of momentum and wavelength are allowed. This is analogous to the postulate for quantum circular motion in the Bohr model of the hydrogen atom. However, for motion along the infinite nanotube length, there is translational symmetry, and consequently the electron wave functions are Bloch running waves in continuous energy bands. Without correlation, the fundamental π to π^* band gap transition (HOMO−LUMO) is delocalized along the entire tube length. The HOMO hole and LUMO electron are eigenfunctions of momentum. The electron moves independently of the hole.

If one now considers correlation, bound neutral exciton states can exist at energies below the band gap, at which free carriers move independently along the entire CNT length. Correlation creates attractive Coulomb interaction between the positive hole and negative excited electron. Attraction for the positive "hole" represents the net effect of repulsion with all the remaining electrons in the valence band. If the Coulomb interaction is strong then the exciton lies far below the band gap. The exciton is a mutually bound electron and hole orbiting each other in correlated motion at a separation of ca. 2 nm (Figure 4). This state is similar to a π−π^* excited state in an aromatic molecule.

Gordana Dukovic, working very closely with Feng Wang and Tony Heinz, measured the strength of the binding by comparing one-photon and two-photon luminescence excitation spectra.[18] The exciton was bound by about 450 meV in the (6,5) tube. This is about a factor of 50 larger than in bulk 3D

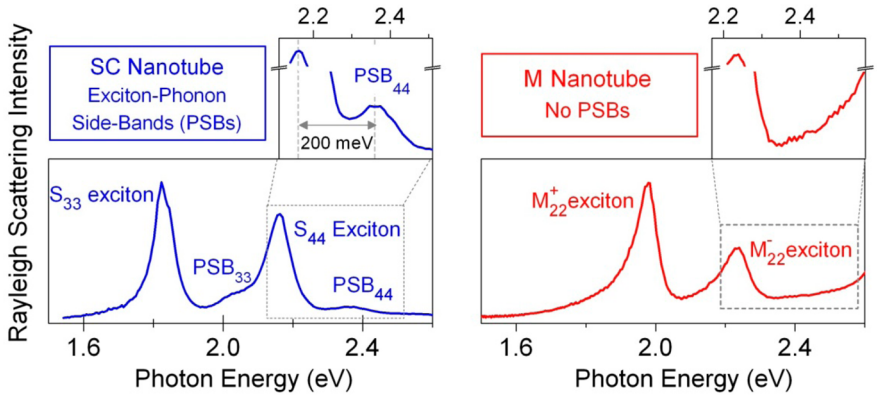

Figure 3. Rayleigh spectra of semiconducing (SC) and metallic (M) SWNTs. Inserts highlight vibronic bands (PSBs) in SC tubes. Reprinted with permission from ref 16. Copyright 2010 American Chemical Society.

dx.doi.org/10.1021/ar500175h | Acc. Chem. Res. 2014, 47, 2951−2959

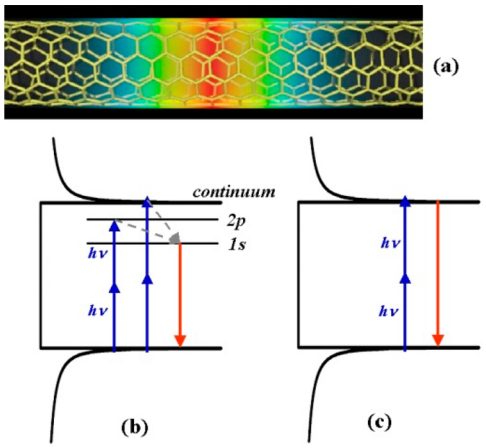

Figure 4. (a) Bound exciton on SWNT. (b) Two photon absorption processes with 1s and 2p excitons. Red fluorescence occurs from the lowest 1s exciton. (c) Hypothetical two photon process without correlation. Reprinted with permission from ref 16. Copyright 2010 American Chemical Society.

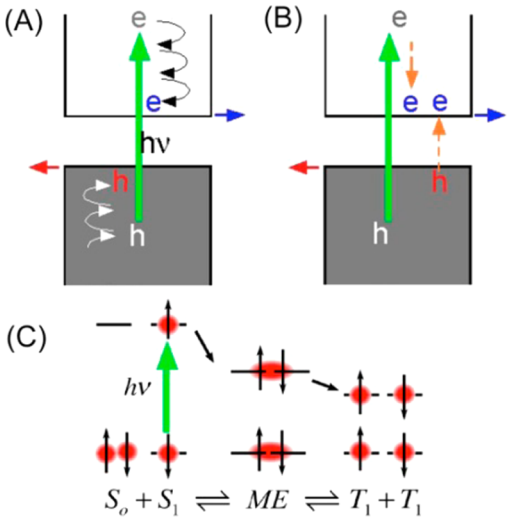

Figure 5. (A) Schematic of hot carrier vibrational relaxation to the band edge creating heat. (B) Hot electron relaxation creating an exciton. Both processes result from absorption of a high energy photon. (C) Molecular orbitals for singlet fission in a pentacene crystal.

semiconductors such as silicon and GaAs. CNT excitons have become an active research area.[19]

Strong correlation also allows individual electrons to decay into multielectron species. For example, a "hot" electron with large kinetic energy, far above the CNT conduction band edge, could decay:

$$e^-(\text{hot}) \rightarrow e^-(\text{band edge}) + \text{an exciton} \quad (1)$$

In this process, one electron becomes two electrons and one hole, thus conserving charge. The process is allowed if energy and momentum are also conserved. This nonradiative electronic transition competes with vibrational cooling of the hot electron to the band edge. In almost all physical systems, hot carriers normally decay by vibrational heat production: indeed this is the process that creates the Shockley–Queisser limit in photovoltaics. A pioneering 2005 experiment by Avouris and co-workers showed that process 1 is amazingly fast in semiconductor CNTs.[20] If an electron is injected and accelerated in a semiconductor CNT with applied source–drain voltage, very strong exciton luminescence created by process 1 occurs. The rate is near 10^{+15} s^{-1},[21] corresponding to a lifetime of only 1 fs. This decay to a multielectron state is as fast as any dynamical process can be in molecular science. In a related experiment (Figure 5), McEuen and co-workers[22] observed that absorption of highly energetic photons, in a similar CNT with applied voltage, led to carrier multiplication with unity quantum yield in the electrical current at low temperature. Baer and Rabani calculated that the initial highly excited exciton decays into a very hot electron in the third transverse conduction band, plus a hole on the valence band edge.[23] Part of the energy to create the very hot electron comes from the initial photon, and part from electron acceleration caused by the applied voltage. This hot electron then generates multiple carriers at a near 10^{+15} s^{-1} rate, as in the Avouris experiment.

These experiments show that correlation is especially strong in semiconductor CNTs. Indeed even in metallic nanotubes, strong correlation causes the absorption spectrum to consist of bound neutral excitons (as we observed by Rayleigh scattering) rather than continuous bands.[24]

Why is correlation so strong in nanotubes? In CNTs, the effective electronic structure is between 2D and 1D, while bulk silicon and GaAs are 3D. Twenty five years ago, the role of pure dimensionality in correlation was first considered,[25] when studies of thin 2D semiconductor GaAs sheets, "quantum wells", showed that excitons were stronger in 2D GaAs than in 3D GaAs. Exciton binding is related to the magnitude of the Coulomb interaction averaged over electron kinetic motion. In 3D GaAs, if one mathematically confines electron–hole motion to a 2D plane, as compared with the natural motion in 3D, the calculated lowest exciton binding energy is four times as large as in 3D. Using the Virial Theorem, the electron–hole Coulomb interaction is also four times as large. If one mathematically confines motion to a line in GaAs, the exciton Coulomb energy diverges.[26] Moving electrons cannot avoid each other in 1D. From this point of view, 1D systems should show maximal electron correlation. (Correlation in 0D quantum dots is weaker as discussed later.) Note also that as the overlap of electron and hole increases in 2D and 1D, the integrated intensity of exciton optical absorption peaks increases. For strong correlation, discrete exciton peaks completely dominate the optical spectra, replacing continuous bands.[27]

There is a second aspect of dimensionality that increases correlation in 2D and 1D: decreased dielectric screening.[28] In bulk 3D semiconductors, screening is strong. In a homogeneous dielectric, the screened Coulomb potential is $e^2/(\varepsilon r)$; thus inside a Si crystal with dielectric constant ε = 11.7, the Coulomb interaction is an order of magnitude weaker than in vacuum. Screening depends upon the neighborhood; it is nonlocal. In CNTs, the sp^2 π electrons are right on the surface. Part of the electric field extending from electron to hole fringes out of the nanotube into the neighborhood. The net screening depends upon the dielectric constant of the surroundings; in vacuum, the effective ε for a semiconductor nanotube is about factor of about four less than that in a 3D silicon crystal. Theoretically, the Coulomb interaction in a 2D dielectric sheet of vanishing thickness has both a short-range, partially screened logarithmic component and a longer unscreened $1/r$

dx.doi.org/10.1021/ar500175h | Acc. Chem. Res. 2014, 47, 2951–2959

component.[29] The Coulomb interaction between electron and hole in a Qdot involves nonlocal image charges that represent the dielectric interface between Qdot and surroundings.[30]

The CNT acts very much as a molecule: properties depend somewhat upon the local environment, and the optical absorption spectrum consists of tightly bound neutral exciton states, rather than continuous bands of free carriers.

Even though 2D graphene is a semimetal and shows broad continuous optical absorption, electron correlation is strong. In the ultraviolet, a short-lived exciton bound by about 400 meV forms at the M saddle point.[31,32] This exciton is embedded in the free carrier bands, and interference creates an asymmetric Fano line shape. Optically excited graphene shows strong carrier multiplication within 100 fs, on a faster time scale than vibrational carrier cooling to the Fermi level.[33,34] This is analogous to similarly fast exciton generation in semiconductor carbon nanotubes. Also, remarkably strong correlation is observed in the graphene ground electronic state, in the presence of an intense perpendicular magnetic field, which causes electrons to orbit in tight circles (Landau levels). This π electron localization removes the effect of kinetic energy and allows full correlation, due to an almost unscreened Coulomb interaction, to form. This coupled π electron ground state shows a robust fractional charge quantum Hall effect, the classic signature of a strongly correlated system, at low temperature.[35,36]

TWO-DIMENSIONAL SHEETS OF LEAD IODIDE PEROVSKITES AND TRANSITION METAL DICHALCOGENIDES

In 1989, Ishihara, Takahasi, and Goto discovered that organic–inorganic lead iodide materials show a striking electron correlation increase in 2D sheets.[37] Three-dimensional bulk $CH_3NH_3PbI_3$ is a cubic perovskite 1.6 eV direct gap semiconductor, in which methylammonium ions balance the charge of $[PbI_6]^{4-}$ octahedra. This material is conveniently processable and recently has found use in efficient solar cells.[38,39] By using longer hydrocarbon counterions, one can synthesize layered 2D versions of 1, 2, and 3 unit cell thickness as van der Waals crystals (Figure 6).[40] These materials luminesce strongly and can be easily exfoliated.[41] Figure 7 compares the optical spectra of the one layer thick $(C_{10}H_{21}NH_3)_2PbI_4$ 2D van der Waals crystal with the cubic 3D parent. While the 3D parent has a very small exciton peak at 1.6 eV with broad continuous bands to high energy, the 2D material has an intense, dominant exciton peak at 2.58 eV, with weaker structured absorption to higher energy.[42,43] This change is a dimensionality effect: the Pb and I orbitals for the valence and conduction bands are similar in 2D and 3D material.[44] In going from 3D to 2D, the band gap increases by about 1 eV due to quantum confinement in the perpendicular direction. The exciton binding energy increases from 37 meV in 3D to 320 meV in 2D.[45] This near 10-fold increase reflects both the factor of 4 kinetic effect discussed above for GaAs, and a substantial decrease in the local dielectric constant in the presence of large hydrocarbon counterions. Figure 8 schematic compares band gaps and exciton binding in 3D and 2D.

Very similar effects occur in thin CdSe platelets made by colloidal chemical synthesis[46] and in 2D transition metal dichalcogenides. Bulk MoS_2 (Figure 9) is a van der Waals crystal of hexagonal sheets exhibiting trigonal prismatic S coordination around Mo atoms. MoS_2 is an indirect gap semiconductor and luminescences weakly in the IR. However,

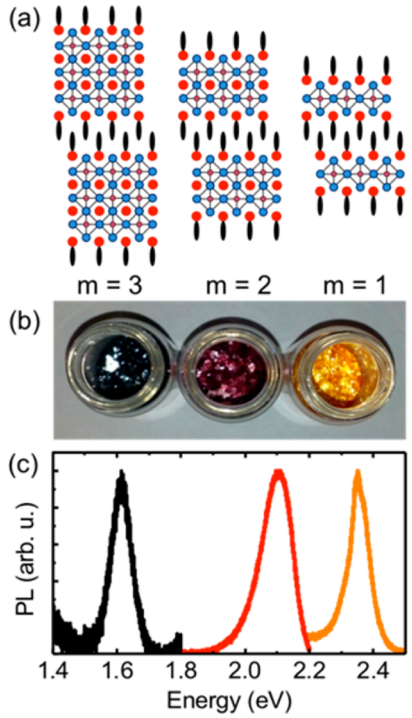

Figure 6. (A) Two-dimensional organic–inorganic Pb iodide perovskites; m is the number of perovskite layers in a 2D structure. (B) Photograph showing material color change with m. (C) Luminescence spectra as a function of m. The m = 3 spectra are similar to the bulk 3D perovskite material. Adapted from ref 41.

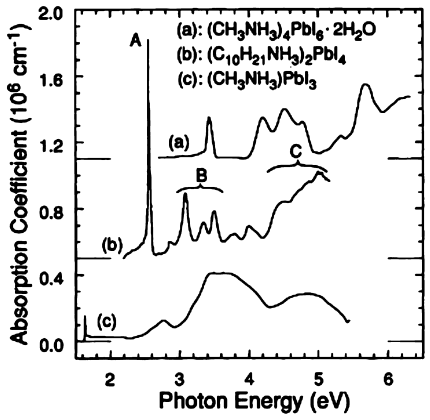

Figure 7. Absorption spectra (4.2 K) of 0, 2, and 3D perovskites. (a) 0D, molecular crystal of individual $(CH_3NH_3)4PbI_6{\cdot}2H_2O$ molecules; (b) 2D, m = 1 layered van der Waals crystal as in Figure 6; (c) 3D, bulk cubic perovskite crystal. Figure from ref 43, reprinted with permission from the Journal of the Physical Society of Japan.

exfoliated single MoS_2 sheets are direct gap and luminesce strongly in the visible.[47,48] Calculation[49] shows that valence band S orbitals at the indirect gap interact from one layer to the next, delocalizing the indirect gap in the perpendicular direction. This delocalization is lost in isolated single sheets, and thus the indirect gap shifts to higher energy, rising above the direct gap. This is a quantum size effect as in 2D lead iodide. States at the direct gap however are formed from crystal-field-split Mo d orbitals and are delocalized in the 2D plane. The direct gap energy is thus insensitive to the number of layers.

dx.doi.org/10.1021/ar500175h | Acc. Chem. Res. 2014, 47, 2951–2959

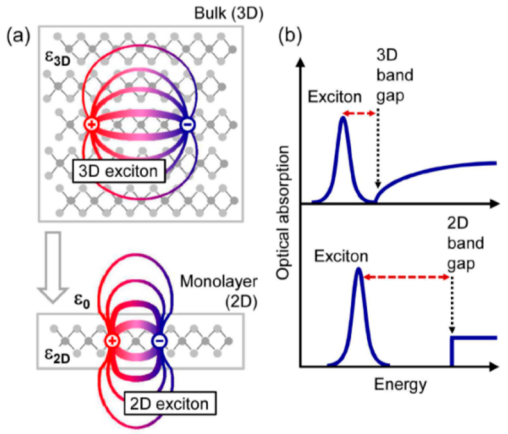

Figure 8. Schematic of increased (a) Coulomb interaction and (b) exciton binding in 2D compared with 3D materials. Adapted from ref 53.

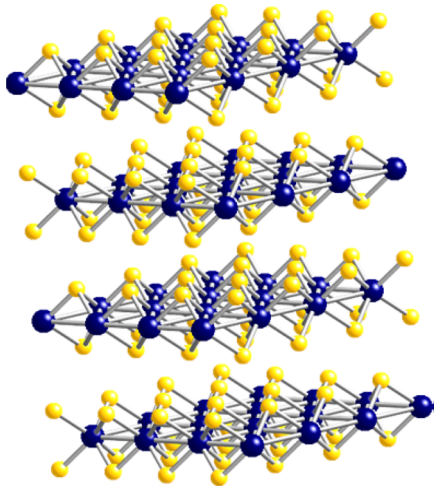

Figure 9. Schematic diagram of four partial layers of MoS_2 van der Waals crystal. S atoms (yellow) exhibit trigonal prismatic coordination around Mo atoms (blue). Figure from Michael Steigerwald.

Single MoS_2 sheets show a pronounced 1.88 eV exciton in both absorption and luminescence: this exciton is split into A and B peaks by the spin−orbit coupling of the valence band. This exciton is tightly localized spatially with a radius of 1 nm and shows an unprecedented ca. 25 meV binding to any free electrons present in the sheet.[50] Such strongly bound trions are another manifestation of strong Coulombic interaction.[51] A recent correlated GW-BSE calculation[52] in Figure 10 also shows several higher excitons, which are lifetime broadened into an apparent continuum as experimentally observed. In supported WS_2 sheets, the lowest exciton is experimentally bound by 320 meV.[53] WS_2 also shows a Rydberg series of higher excitons whose relative spacing indicates that the Coulomb attraction deviates from the simple $1/r$ hydrogenic potential, as discussed earlier for 2D sheets.

■ QUANTUM DOTS AND MOLECULES

Zero dimensional (0D) quantum dots (Qdots, Figure 1) of sp^3 semiconductors have discrete energy levels and essentially are large molecules.[54] Qdot electron and hole wave functions have nodes on the Qdot surface; the electron and hole are both "inside", and thus the Coulomb interaction is strongly screened,

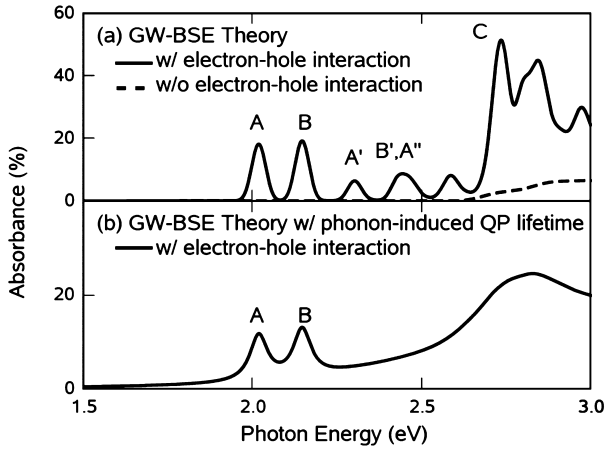

Figure 10. GW-BSE correlated calculation of single sheet MoS_2 optical spectra. Panel a shows spectra with and without correlation creating excitons. Panel b shows the predicted spectra including calculated fast vibrational cooling, which makes the discrete structure of the higher excitons appear to be a continuum. Panel b is close to the experimental spectrum. Figure from Professor Steven Louie at Berkeley.

similar to 3D bulk semiconductors. A 4 nm CdSe Qdot is calculated to have a relative dielectric constant within 10% of the bulk 6.2 value.[55] True excitons, that is, correlated electron−hole pairs bound solely by their Coulomb attraction, do not form in 4 nm Qdots. The lowest 1s exciton spatial (quantum confined) pattern is fixed by the Qdot size and shape; this is analogous to a molecular orbital spatial pattern being determined by atom positions. The individual quantum confinements of electron and hole add to shift the excited state to higher energy than the bulk band gap. The net Coulomb interaction between electron and hole stabilizes the excited state energy by a few tenths of an eV but does not induce correlated electron−hole relative motion or strongly mix this lowest 1s excited state with other states. This state is more like a molecular excited state. Nevertheless, Qdot excited states are historically labeled "excitons".

A 4 nm Qdot contains about a thousand atoms; consequently the density of excited electronic states increases extremely rapidly with energy. At energies about three times the band gap, single excitons are always degenerate with two or more excitons based upon lower energy electrons and holes. Correlation allows the Qdot single energetic exciton to decay irreversibly into these two band gap excitons in the multiple exciton generation (MEG) process.[56−58] Modest MEG efficiencies reaching 30% at energies near three times the scaled band gap have been observed.[59] Stochastic Fermi Golden Rule calculations suggest that MEG occurs due to extremely high densities of degenerate multiexciton states,[60,61] even though the Coulomb interaction is strongly screened.

Qdot MEG produces two excitons from one high energy photon. The fact that one Qdot can contain two excited states is another consequence of large size: this does not occur in molecules. However, the second exciton is short-lived as two relaxed excitons, confined in the same Qdot, interact and decay by Auger recombination, which is essentially the inverse of the original MEG process. On the other hand, one exciton is stable in a well-made core/shell Qdot. Such Qdots have near unity luminescence quantum yields, can survive billions of excitation/emission cycles, and show vivid emission colors. Red and green

dx.doi.org/10.1021/ar500175h | Acc. Chem. Res. 2014, 47, 2951−2959

luminescent Qdots have been used for display in Sony TVs and Kindle tablets.

Strong correlation appears from states that are near degenerate. In small molecules, states are sparse, and accidental degeneracies are rare. When two or a few zero-order states are degenerate, correlation creates coherent mixing, as occurs in short polyenes to be described below and in short tubular aromatic molecules based upon the (5,5) metallic carbon nanotube.[62] Polyacene van der Waals crystals show correlation-induced excited singlet fission into two triplets on neighboring molecules.[63−65] In pentacene, there is close degeneracy between the triplet pair and the excited singlet (Figure 5); fission occurs within 70−100 fs. The initial singlet excited state is delocalized over several molecules, and has partial charge transfer character. Zhu and co-workers showed that the initial singlet is coupled to an intermediate multiexciton state.[66,67] This occurs indirectly through charge transfer states with an effective strength of ca. 200 meV.[68−70] The intermediate state quickly decays into two relaxed triplets that are independently mobile in the crystal.

SOLITONS IN POLYACETYLENE

As a final example, we discuss the remarkable, purely 1D π electron system of linear all-*trans* polyacetylene (PA). In a simple Huckel treatment with equal bond lengths, infinite PA is a metal with a half filled band. Such a 1D metal is unstable under Jahn−Teller (Peierls) distortion, and thus PA actually is a semiconductor with alternating short and long bonds. Such a 1D semiconductor should show very strong exciton effects, and correlated GW calculations do show that the optical spectrum is completely dominated by one neutral exciton sitting about 400 meV below the band gap, which itself is not apparent in the spectrum.[71]

It has long been understood that strong correlation is important in excited states of short linear conjugated polyene molecules.[72] As chain length increases beyond butadiene,[73] a nonluminescent A_g state drops below the optically allowed B_u state. In octatetraene, for example, this A_g state is a mixture of singly and doubly excited configurations and requires a multideterminant, explicitly correlated wave function.[74] This is the beginning of the strong correlation seen in the infinite PA chain.

Polyacetylene also exhibits a unique "soliton" correlated state not seen in the examples above. Su, Schrieffer, and Heeger[75] predicted that the vibrational mode that interchanges short and long bonds would create a "soliton" vibronic state, as shown in Figure 11, inside the band gap. Consider a PA chain in which a

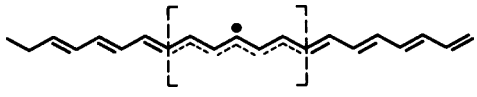

Figure 11. Soliton junction between domains in polyacetylene. The dot is an unpaired p electron. Note that the double bonds have opposite phases left and right of the junction.

short section has reversed long/short bonds with respect to the parent chain. This section (or domain) will have two interfaces with the main chain, at each of which there will be one carbon atom with an unpaired p electron. These two interface regions are solitons. Solitons contain an odd number of sp^2 carbons and thus are neutral yet show spin 1/2. They are an excitation of the ground state chain showing uniform long/short bond alternation. When close together, the two solitons interact to form an excited singlet or triplet state, analogous to a normal molecular excited state. In fact, Taven and Schulten have argued that the lowest PA ^1A_g covalent excited state could spontaneous separate into two components.[76]

Separated solitons are independently mobile along the chain. Because the long/short bond length difference is not large, the soliton boundary region moves with an effective mass calculated to be about 6 times an electron mass. Separated solitons represent promotion of effectively one-half electron each.

The exciton, and even relaxed individual electrons and holes at the band edges, are not stable in PA.[77] A valence band hole decays into a soliton at lower energy. The initial hole has positive charge and spin 1/2. The ionized soliton produced by hole decay has positive charge and spin zero. (Charged solitons are odd alternate hydrocarbon ions in organic chemistry.[78]) The spin is zero because the unpaired p electron is gone. The nearby π electrons are paired up across the short bonds with opposite phases to the left and right of the junction. In PA chemically hole doped by adsorbed halogens, mobile charged solitons (carbonium ions) carry current along the chain. When PA is optically excited, the initial exciton decays into two solitons of opposite charge within 250 fs.[79] Thus, PA solitons effectively separate electron spin and charge and show behavior expected of fractional charge.[80]

While CNTs and graphene do not show bond alternation, graphene armchair edges naturally impose some local bond alternation. A large graphene structure in the shape of a hexagon with armchair edges is predicted to show fixed solitons at its six vertices, which effectively act as boundaries between armchair edges of different bond phases.[81] Solitons involve unpaired single p electrons at mobile zone boundaries. Zigzag edges on graphene also have localized nonbonding p electrons that couple together to form biradical-type magnetic edge states, as studied in the model compound quarteranthene[82]

FINAL COMMENTS ON STRONG ELECTRON CORRELATION

In 1D and 2D materials, an electronic band structure diagram by itself can be misleading if one does not consider explicit correlation. In strictly 1D systems, electrons cannot move in ways to avoid collisions with each other. Thus, a 1D metal is very strongly correlated; we have seen above how metallic CNT spectra are dominated by excitons. In addition, electrical conductivity does not obey the simple free electron model valid in 3D metals such as Cu or Pt. McEuen, Smalley, and co-workers showed that π electrons in metallic CNTs conduct electricity as predicted by a correlated Luttinger model, in which charge and spin effectively separate.[83,84] This is similar to the quantum Hall effect and the soliton.

The correlated soliton structure is logical, being rooted in valence bond ideas about local electron pairing. Local pairing is at the heart of "electron pushing" reaction mechanisms in organic chemistry. The valence bond approach is naturally correlated. Valence bond, Hubbard, and Pariser−Parr−Pople (PPP) theories all offer increased electron−electron repulsion over that present in Hartree−Fock molecular orbital wave functions.[85] These simplified models all offer insight, but it is very hard to do accurate systematic calculations on large systems.

The correlated exciton in 1D and 2D systems is also logical, being rooted in the idea of a bound state formed from orbiting

charges of opposite sign. This simple model gives nearly quantitative results. In forming an exciton, the Coulomb interaction creates a localized Fourier transform of spatially delocalized band states. As delocalization becomes weaker, a deeper and tighter bound exciton is formed. The MoS_2 family shows remarkably strong exciton effects. Here the 2D conduction and valence bands are both composed of crystal-field-split Mo d orbitals, which typically show weak effective Mo−Mo bonding and thus modest kinetic delocalization.

When kinetic delocalization is not large, the Coulomb repulsion is relatively more important and can even dominate as occurs in Mott insulator solids. Strong correlation can create exotic electrical and magnetic phase diagrams. Decades of intense research has led to partial understanding of strongly correlated solids.[86−88] New theoretical approaches are being implemented.[89−91] The GW-BSE approximation often accurately predicts excitonic optical spectra.[92]

The full complexity of strong correlation is revealed in high-temperature superconductors containing transition metals. Complexity is often associated with 2D bonding at the Fermi level, such as in the copper oxide $La_{2-x}Sr_xCuO_4$ and iron pnictide $LaFeAsO_{1-x}F_x$ families. Many fundamental questions remain open, and there is little predictive ability at present. Superconductivity involves mobile singlet electron pairs carrying current. Indeed, one early theory of high temperature superconductivity was inspired by Linus Pauling's idea of resonating valence bonds.[93]

AUTHOR INFORMATION

Corresponding Author

*E-mail: leb26@columbia.edu.

Notes

The authors declare no competing financial interest.

Biography

Louis Brus was a scientist in AT&T Bell Laboratories, Murray Hill, NJ, before joining the Columbia chemistry faculty in 1996. He was Chairman of the Board of Trustees for the Gordon Research Conferences in 1998. He has received the Kavli Prize in nanoscience and the Welch Prize in chemistry.

ACKNOWLEDGMENTS

We thank the referees for insightful suggestions. We also thank David Reichman, Eran Rabani, Mark Hybertsen, Mike Steigerwald, Xiaoyang Zhu, Tony Heinz, Sasha Efros, Jim Yardley, Ed Chandross, Tim Berkelbach, Alexey Chernikov, and Omer Yaffe for stimulating discussions. This work is supported by DOE Basic Energy Sciences in the Columbia Energy Frontier Research Center under Award DE-SC0001085.

REFERENCES

(1) Iijima, S. Helical microtubules of graphitic carbon. *Nature* **1991**, *354*, 56−58.

(2) Mintmire, J.; W. Dunlap, B. I.; White, C. T. Are fullerene tubes metallic? *Phys. Rev. Lett.* **1992**, *68*, 631−634.

(3) Saito, R.; Fujita, M.; Dresselhaus, G.; Dresselhaus, M. S. Electronic structure of graphene tubules based upon C_{60}. *Phys. Rev. B* **1992**, *46*, 1804−1811.

(4) Novoselov, K. S.; Geim, A. K.; Morozov, S. V.; Jiang, D.; Zhang, Y.; Dubonos, S. V.; Gigorieva, I. V.; Firsov, A. A. Electric field effect in atomically thin carbon films. *Science* **2004**, *306*, 666−669.

(5) Macklin, J. J.; Trautman, J. K.; Harris, T. D.; Brus, L. E. Imaging and time-resolved spectroscopy of single molecules at an interface. *Science* **1996**, *272*, 255−258.

(6) Nirmal, N.; Dabbousi, B. O.; Bawendi, M. G.; Macklin, J. J.; Trautman, J. K.; Harris, T. D.; Brus, L. E. Fluorescence intermittency of single cadmium selenide nanocrysals. *Nature* **1996**, *383*, 802−805.

(7) O'Connell, M. J.; Bachilo, S. M.; Huffman, C. B.; Moore, V. C.; Strano, M. S.; Haroz, E. H.; Rialon, K. L.; Boul, P. J.; Noon, W. N.; Kittrell, C.; Ma, J.; Hauge, R. H.; Weisman, R. B.; Smalley, R. E. Band gap fluorescence from individual single-walled carbon nanotubes. *Science* **2002**, *297*, 593−596.

(8) Michaels, A. M.; Nirmal, M.; Brus, L. E. Surface enhanced Raman spectroscopy of individual R6G molecules on large Ag nanocrystals. *J. Am. Chem. Soc.* **1999**, *121*, 9932−9938.

(9) Brus, L. Noble metal nanocrystals: Plasmon electron transfer photochemistry and single molecule raman spectroscopy. *Acc. Chem. Res.* **2008**, *41*, 1742−1747.

(10) Yu, Z.; Brus, L. Rayleigh and Raman scattering from individual carbon nanotube bundles. *J. Phys. Chem. B* **2001**, *105*, 1123−1129.

(11) Sfeir, M. Y.; Wang, F.; Huang, L.; Chuang, C.; Hone, J.; O'Brien, S.; Heinz, T. F.; Brus, L. E. Probing electronic transitions of individual carbon nanotubes by Rayleigh scattering. *Science* **2004**, *306*, 1540−1543.

(12) Wang, F.; Sfeir, M.; Huang, L.; Huang, X. M.; Wu, Y.; Kim, J.; Hone, J.; O'Brien, S.; Brus, L.; Heinz, T. Interactions between individual carbon nanotubes studied by Rayleigh scattering spectroscopy. *Phys. Rev. Lett.* **2006**, *96*, No. 167401.

(13) Sfeir, M.; Beetz, T.; Wang, F.; Huang, L.; Huang, X. M. H.; Huang, M.; Hone, J.; O'Brien, P.; Misewich, J.; Heinz, T.; Wu, L.; Zhu, Y.; Brus, L. Optical spectroscopy of individual single-walled carbon nanotubes of defined chiral structure. *Science* **2006**, *312*, 554−556.

(14) Berciaud, S.; Voisin, C.; Yan, H.; Chandra, B.; Caldwell, R.; Shan, Y.; Brus, L.; Hone, J.; Heinz, T. Excitons and high-order optical transitions in individual carbon nanotubes: A Rayleigh scattering Spectroscopic Study. *Phys. Rev. B* **2010**, *81*, No. 041414(R).

(15) Liu, K.; Deslippe, J.; Xiao, F.; Capaz, R.; Hong, X.; Aloni, S.; Zettl, A.; Wang, W.; Bai, X.; Louie, S.; Wang, E.; Wang, F. An Atlas of carbon nanotube optical transitions. *Nat. Nanotechnol.* **2012**, *7*, 325−329.

(16) In an earlier note, celebrating the 10th anniversary of *Nano Letters*, we briefly discussed some aspects of correlation: Brus, L. Commentary: Carbon nanotubes, CdSe nanocrystals, and electron−electron interaction. *Nano Lett.* **2010**, *10*, 363−365.

(17) Ando, T. Excitons in carbon nanotubes. *J. Phys. Soc. Jpn.* **1997**, *66*, 1066−1073.

(18) Wang, F.; Dukovic, G.; Brus, L.; Heinz, T. The optical resonances of carbon nanotubes are excitons. *Science* **2005**, *308*, 838−841.

(19) Miyauchi, Y. Photoluminescence studies on exciton photophysics in carbon nanotubes. *J. Mater. Chem. C* **2013**, *1*, 6499−6521.

(20) Chen, J.; Perebeinos, V.; Freitag, M.; Tsang, J.; Fu, Q.; Liu, J.; Avouris, P. Bright infrared emission from electrically induced excitons in carbon nanotubes. *Science* **2005**, *310*, 1171−1173.

(21) Perebeinos, V.; Avouris, P. Impact excitation by hot carriers in carbon nanotubes. *Phys. Rev. B* **2006**, *74*, No. 121410R.

(22) Gabor, N.; Zhong, Z.; Bosnick, K.; Park, J.; McEuen, P. Extremely efficient multiple electron-hole pair generation in carbon nanotube photodiodes. *Science* **2009**, *325*, 1367−1371.

(23) Baer, R.; Rabani, E. Can impact ionization explain efficient carrier multiplication in carbon nanotube photodiodes? *Nano Lett.* **2010**, *10*, 3277−3282.

(24) Deslippe, J.; Spataru, C.; Prendergast, D.; Louie, S. Bound excitons in metallic single-walled carbon nanotubes. *Nano Lett.* **2007**, *7*, 1626−1630.

(25) Schmitt-Rink, S.; Chemla, D.; Miller, D. A. B. Linear and nonlinear optical properties of semiconductor quantum wells. *Adv. Phys.* **1989**, *38*, 89−188.

(26) Loudon, R. One-dimensional hydrogen atom. *Am. J. Phys.* **1959**, *27*, 649−655.

(27) This was first derived in the case of 3D semiconductors in high magnetic field: Elliott, R.; Loudon, R. Theory of the absorption edge in semiconductors in a high magnetic field. *J. Phys. Chem. Solids* **1960**, *15*, 196−207.
(28) This was first recognized for 2D systems in Keldysh, L. Coulomb interaction in thin semiconductor and semimetal films. *JETP Lett.* **1979**, *29*, 658−661.
(29) Cudazzo, P.; Tokatly, I.; Rubio, A. Dielectric screening in two-dimensional insulators: Implications for excitonic and impurity states in graphene. *Phys. Rev. B* **2011**, *84*, No. 085406.
(30) (a) Brus, L. A simple model for the ionization potential, electron affinity, and aqueous redox potentials of small semiconductor crystallites. *J. Chem. Phys.* **1983**, *79*, 5566−5571. (b) Brus, L. Electron-electron and electron-hole interactions in small semiconductor crystallites: The size dependence of the lowest excited electronic state. *J. Chem. Phys.* **1984**, *80*, 4403−4408.
(31) Chae, D.; Utikal, T.; Weisenburger, S.; Giessen, S.; v. Klitzing, K.; Lippitz, M.; Smet, J. Excitonic Fano resonance in free-standing graphene. *Nano Lett.* **2011**, *11*, 1379−1382.
(32) Mak, F.; Shan, J.; Heinz, T. Seeing many-body effects in single- and few-layer graphene: observation of two-dimensional saddle point excitons. *Phys. Rev. Lett.* **2011**, *106*, No. 046401.
(33) Brida, D.; Tomadin, A.; Manzoni, C.; Kim, Y.; Lombardo, A.; Milana, S.; Nair, R.; Novoselov, K.; Ferrari, A.; Cerullo, G.; Polini, M. Ultrafast collinear scattering and carrier multiplication in graphene. *Nat. Commun.* **2013**, *4*, No. 1987.
(34) Tielrooij, K.; Song, J.; Jensen, S.; Centeno, A.; Pesquera, A.; Zurutuza Elorza, A.; Bonn, M.; Levitov, L.; Koppens, F. Photo-excitation cascade and multiple carrier generation in graphene. *Nat. Phys.* **2013**, *9*, 248−252.
(35) Bolotin, K.; Gharhari, F.; Schulman, M.; Stormer, H.; Kim, P. Observation of the fractional quantum Hall effect in graphene. *Nature* **2009**, *462*, 196−199.
(36) Du, X.; Skachko, I.; Duerr, F.; Luican, A.; Andrei, E. Fractional quantum Hall effect and insulating phase of Dirac electrons in graphene. *Nature* **2009**, *462*, 192−195.
(37) Ishihara, T.; Takahashi, J.; Goto, T. Exciton state in two-dimensional perovskite semiconductor $(C_{10}H_{21}NH_3)_2PbI_4$. *Solid State Commun.* **1989**, *69*, 933−936.
(38) Xing, G.; Mathews, N.; Sun, S.; Lim, S.; Lam, Y.; Gratzel, M.; Mhaisalkar, S.; Sum, T. Long range balanced electron and hole-transport lengths in organic-inorganic $CH_3NH_3PbI_3$. *Science* **2013**, *342*, 344−347.
(39) Stranks, S.; Eperon, G.; Grancini, G.; Menetaou, C.; Alcocer, M.; Leijtens, T.; Herz, L.; Petrozza, A.; Snaith, H. Electron-hole diffusion lengths exceeding 1 micrometer in an organometal trihalide perovskite absorber. *Science* **2013**, *342*, 341−344.
(40) Mitzi, D. Synthesis, structure and properties of organic-inorganic perovskites and related materials. *Prog. Inorg. Chem.* **1999**, *48*, 1−121.
(41) Yaffe, O.; Chernikov, A.; Norman, Z.; Zhong, Y.; Velauthapillai, A.; van der Zande, A.; Owen, J.; Heinz. T. A New Hybrid 2D material; ultrathin organic-inorganic perovskites crystals. Manuscript in preparation, 2014.
(42) Hong, X.; Ishihara; Nurmikko, A. Dielectric confinement effect on excitons in PbI4-based layered semiconductors. *Phys. Rev. B* **1992**, *45*, 6991−6994.
(43) Hirasawa, M.; Ishihara, T.; Goto, T. Exciton features in 0-, 2-, and 3-dimensional networks of [PbI6]4- octahedra. *J. Phys. Soc. Jpn.* **1994**, *63*, 3870−3879.
(44) Umebayashi, T.; Asai, K.; Kondo, T.; Nakao, A. Electronic structures of lead iodide low-dimensional crystals. *Phys. Rev. B* **2003**, *67*, No. 155405.
(45) Hirasawa, M.; Ishihara, T.; Goto, T.; Uchida, K.; Miura, N. Magnetoabsorption of the lowest exciton in perovskite-type compound CH_3NH_3PbI. *Physica B* **1994**, *201*, 427−430.
(46) Benchamekh, R.; Gippius, N.; Even, J.; Nestoklon, M.; Jancu, J.-M.; Ithurria, S.; Dubertret, B.; Efros, Al.; Voisin, P. Tight-binding calculations of image-charge effects in colloidal nanoscale platlets of CdSe. *Phys. Rev. B* **2014**, *89*, No. 035307.
(47) Mak, K.; Lee, C.; Hone, J.; Shan, J.; Heinz, T. Atomically thin MoS_2: A new direct-gap semiconductor. *Phys. Rev. Lett.* **2010**, *105*, No. 136805.
(48) Splendiana, A.; Sun, L.; Zhang, Y.; Li, T.; Kim, J.; Chim, C.-Y.; Galli, G.; Wang, F. Emerging photoluminescence in monolayer MoS_2. *Nano Lett.* **2010**, *10*, 1271−1276.
(49) Li, T.; Galli, G. Electronic properties of MoS_2 nanoparticles. *J. Phys. Chem. C* **2007**, *111*, 16192−16196.
(50) Mak, K.; He, K.; Lee, C.; Lee, G.; Hone, J.; Heinz, T.; Shan, J. Tightly bound trions in monolayer MoS2. *Nat. Mater.* **2013**, *12*, 207−211.
(51) Berkelbach, T.; Hybertsen, M.; Reichman, D. Theory of neutral and charged excitons in monolayer transition metal dichalcogenides. *Phys. Rev. B* **2013**, *88*, No. 045318.
(52) See Qiu, D.; da Jornada, F.; Louie, S. Optical spectrum of MoS_2: Many body effects and diversity of exciton states. *Phys. Rev. Lett.* **2013**, *111*, No. 216805, and references contained therein..
(53) Chernikov, A.; Berkelbach, T.; Hill, T.; Rigosi, A.; Li, Y.; Aslan, O.; Reichman, D.; Hybertsen, M.; Heinz, T. Non-hydrogenic Rydberg series and exciton binding energy in monolayer WS_2. *Phys. Rev. Lett.* **2014**, in press.
(54) Brus, L. Electronic wave functions in semiconductor clusters: experiment and theory. *J. Phys. Chem.* **1986**, *90*, 2555−2560.
(55) Wang, L.-W.; Zunger, A. Pseudopotential calculations of nanoscale CdSe quantum dots. *Phys. Rev. B* **1996**, *53*, 9579−1982.
(56) Schaller, R.; Agranovich, V.; Klimov, V. High-effeciency carrier multiplication through direct photogeneration of multi-excitons via virtual single-exciton states. *Nat. Phys.* **2005**, *1*, 189−194.
(57) Shabaev, A.; Efros, A.; Nozik, A. Multiexciton generation by a single photon in nanocrystals. *Nano Lett.* **2006**, *6*, 2856−2863.
(58) Padilha, L.; Stewart, J.; Sandberg, R.; Bae, W.; Koh, W.-K.; Pietryga, J.; Klimov, V. Carrier multiplication in semiconductor nanocrystals: Influence of size, shape and composition. *Acc. Chem. Res.* **2013**, *46*, 1261−1269.
(59) Nair, G.; Chang, L.-Y.; Geyer, S.; Bawendi, M. Perspective on the prospects of a carrier multiplication nanocrystal solar cell. *Nano Lett.* **2011**, *11*, 2145−2151.
(60) Baer, R.; Rabani, E. Expeditious stochastic calculation of multiexciton generation rates in semiconductor nanocrystals. *Nano Lett.* **2012**, *12*, 2123−2128.
(61) Zohar, G.; Baer, R.; Rabani, E. Mutiexciton generation in IV-IV nanocrystals: The role of carrier effective mass, band mixing, and phonon emission. *J. Phys. Chem. Lett.* **2013**, *4*, 317−322.
(62) Zhou, Z.; Steigerwald, M.; Hybertsen, M.; Brus, L.; Friesner, R. Electronic structure of tubular organic molecules derived from the metallic (5,5) armchair single wall carbon nanotube. *J. Am. Chem. Soc.* **2004**, *126*, 3597−3605.
(63) Pope. M.; Swenberg, C. *Electronic Processes in organic Crystals and Polymers*, 2nd ed.; Oxford University Press; New York, 1999; pp 1−1328.
(64) Smith, M.; Michl, J. Singlet Fission. *Chem. Rev.* **2010**, *110*, 6891−6936.
(65) Wilson, M.; Rao, A.; Ehrler, B.; Friend, R. Singlet exciton fission in polycrystalline pentacene: From photophysics to devices. *Acc. Chem. Res.* **2013**, *46*, 1330−1338.
(66) Chan, W.-L.; Ligges, M.; Jailaubekov, A.; Kaake, L.; Miaja-Avila, L.; Zhu, X.-Y. Observing the multiexciton state in singlet fission and ensuing ultrafast multielectron transfer. *Science* **2011**, *334*, 1541−1545.
(67) Chan, W.-L.; Ligges, M.; Zhu, X.-Y. The energy barrier in singlet fission can be overcome through coherent coupling and entropic gain. *Nat. Chem.* **2012**, *4*, 840−845.
(68) Chan, W.-L.; Berkelbach, T.; Provorse, M.; Monahan, N.; Tritsch, J.; Hybertsen, M.; Reichman, D.; Gao, J.; Zhu, X.-Y. The Quantum coherent mechanism for singlet fission: Experiment and theory. *Acc. Chem. Res.* **2013**, *46*, 1321−1329.
(69) Greyson, E.; Vura-Weis, J.; Michl, J.; Ratner, M. Maximizing singlet fission in organic dimers: Theoretical investigation of triplet

yield in the regime of localized excitation and fast coherent electron transfer. *J. Phys. Chem. B* **2010**, *114*, 14168−14177.
(70) Berkelbach, T.; Hybertsen, M.; Reichman, D. Microscopic theory of singlet exciton fission. 1 General Formulation. *J. Chem. Phys.* **2013**, *138*, No. 114102.
(71) Rohlfing, M.; Louie, S. Optical excitations in conjugated polymers. *Phys. Rev. Lett.* **1999**, *82*, 1959−1963.
(72) Kohler, B. E. Octatetraene photoisomerization. *Chem. Rev.* **1993**, *93*, 2335−2375.
(73) Watson, M.; Chan, G. K-L. Excited states of butadiene to chemical accuracy: Reconciling theory and experiment. *J. Chem. Theory Comput.* **2012**, *8*, 4013−4018.
(74) Bredas, J. L.; Cornil, J.; Beljonne, D.; Dos Santos, D.; Shuai, Z. Excited state electronic structure of conjugated oligomers and polymers: A quantum chemical approach to optical phenomena. *Acc. Chem. Res.* **1999**, *32*, 267−276.
(75) Su, W.; Schrieffer, J.; Heeger, A. Soliton excitations in polyacetylene. *Phys. Rev. B* **1980**, *22*, 2099−2111.
(76) Tavan, P.; Schulten, K. Electronic excitations in finite and infinite polyenes. *Phys. Rev. B* **1987**, *36*, 4337−4358.
(77) Su, W.; Schrieffer, J. Soliton dynamics in polyacetylene. *Proc. Natl. Acad. Sci. U.S.A.* **1980**, *77*, 5652−5629.
(78) Tolbert, L. Solitons in a box: The organic chemistry of electrically conducting polyenes. *Acc. Chem. Res.* **1992**, *25*, 561−568.
(79) Miranda, P. B.; Moses, D.; Park, Y. K.; Heeger, A. J. Excitation spectrum for ultrafast photogeneration of charged solitons in polyacetylene. *Synth. Met.* **2003**, *135*−*136*, 445−446.
(80) Anderson, P. When the electron falls apart. *Phys. Today* **1997**, 42−47.
(81) Romanovksy, I.; Yannouleas, C.; Landmann, U. Topological effects and particle physics analogies beyond the massless Dirac-Weyl fermion in graphene nanorings. *Phys. Rev. B* **2013**, *87*, No. 165431.
(82) Konishi, A.; Hirao, Y.; Matsumoto, K.; Kurata, H.; Kishi, R.; Shigeta, Y.; Nakano, M.; Tokunaga, K.; Kamada, K.; Kubo, T. Synthesis and characterization of quarteranthene: Elucidating the characteristics of the edge state of graphene nanoribbons at the molecular level. *J. Am. Chem. Soc.* **2013**, *135*, 1430−1437.
(83) Bockrath, M.; Cobden, D.; Lu, J.; Rinzler, A.; Smalley, R.; Balents, L.; McEuen, P. Luttinger-liquid behavior in carbon nanotubes. *Nature* **1999**, *397*, 598−601.
(84) Kane, C.; Balents, L.; Fisher, M. Coulomb interactions and mescopic effects in carbon nanotubes. *Phys. Rev. Lett.* **1997**, *79*, 5086−5089.
(85) Ramasesha, S.; Soos, Z. G. Valence Bond Theory of Quantum Cell Models. In *Valence Bond Theory*; Cooper, D., Ed.; Theoretical and Computational Chemistry, Vol *10*; Elsevier: Amsterdam, 2002, Chapter 20. Schmalz, T. A Valence Bond View of Fullerenes. In *Valence Bond Theory*; Cooper, D., Ed.; Theoretical and Computational Chemistry, Vol *10*; Elsevier: Amsterdam, 2002, Chapter 17.
(86) Gull, E.; Parcollet, O.; Millis, A. Superconductivity and the pseudogap in the two-dimensional Hubbard model. *Phys. Rev. Lett.* **2013**, *110*, No. 216405.
(87) Morosan, E.; Natelson, D.; Nevidomsky, A.; Si, Q. Strongly correlated materials. *Adv. Mater.* **2012**, *23*, 4896−4923.
(88) Basov, D.; Averitt, R.; van der Marel, D.; Dressel, M.; Haule, K. Electrodynamics of correlated electron materials. *Rev. Mod. Phys.* **2011**, *83*, 472−525.
(89) White, S. Density matrix formulation for quantum renormalization groups. *Phys. Rev. Lett.* **1992**, *69*, 2663−2666.
(90) Georges, A.; Kotliar, G.; Krauth, W.; Rozenberg, M. Dynamical mean-field theory of strongly correlated fermion systems and the limit of infinite dimensions. *Rev. Mod. Phys.* **1996**, *68*, 13−124.
(91) Stella, L.; Attaccelite, C.; Sorella, S.; Rubio, A. Strong electronic correlation in the hydrogen chain: A variational Monte Carlo study. *Phys. Rev. B* **2011**, *84*, No. 245117.
(92) Hybertsen, M.; Louie, S. Electron correlation in semiconductors and insulators: Band gaps and quasiparticle energies. *Phys. Rev. B* **1986**, *34*, 5390−5413.
(93) Anderson, P. The resonating valence bond state in La_2CuO_4 and superconductivity. *Science* **1987**, *235*, 1196−1198.